J. Fluid Mech. (1993), *vol.* 246, *pp.* 197–223

Turbulence measurements in axisymmetric jets of air and helium. Part 1. Air jet

By N. R. PANCHAPAKESAN AND J. L. LUMLEY

Sibley School of Mechanical and Aerospace Engineering, Cornell University,
Ithaca, NY 14850, USA

(Received 13 March 1991 and in revised form 29 June 1992)

A turbulent round jet of air discharging into quiescent air was studied experimentally. Some $\times$-wire hot-wire probes mounted on a moving shuttle were used to eliminate rectification errors due to flow reversals in the intermittent region of the jet. Moments of velocity fluctuations up to fourth order were measured to characterize turbulent transport in the jet and to evaluate current models for triple moments that occur in the Reynolds stress equations. Fourth moments were very well described in terms of second moments by the quasi-Gaussian approximation across the entire jet including the intermittent region. Profiles of third moments were found to be significantly different from earlier measurements: $\langle uv^2\rangle$, $\langle uw^2\rangle$ and $\langle u^2v\rangle$ are found to be negative near the axis of the jet. The *Basic* triple moment model that included turbulent production and models for the dissipation and the return-to-isotropy part of the pressure correlations was found to be unsatisfactory. When mean-strain production and a model for rapid pressure correlations were also included, predictions were satisfactory in the fully turbulent region. The consistency of the measurements with the equations of motion was assessed: momentum flux across the jet was found to be within $\pm 5\%$ of the nozzle input and the integral of radial diffusive flux of turbulent kinetic energy across the jet calculated from the measured third moments was found to be close to zero.

1. Introduction

Models that attempt to predict complex turbulent flows need to be evaluated using measurements in basic flows before they can be applied to unknown flows. The turbulent round jet is a simple inhomogeneous flow that serves as a simple model for more complex flows. Prediction methods for complex turbulent flows with swirl, separation, recirculation, curvature and body force effects etc. currently lean towards second-order closures because pressure effects and nonlinear turbulence interactions are found to be important and these effects are not accounted for in simpler closure schemes. In second-order closures turbulent flows are described using the Reynolds stress equations with models for the unclosed terms: pressure-gradient–velocity correlations, dissipation and triple moments (see Lumley 1978). Models for the first two have been extensively tested and refined while testing of models for triple moments has been hampered by a dearth of measurements of higher-order moments in basic flows. In this paper measurements in a turbulent air jet that provide a basis for evaluation of models for triple moments are described.

Turbulent round jets have been studied extensively. Wygnanski & Fiedler (1969, hereafter referred to as W & F) performed a comprehensive study of the self-similar region of the round jet and reported moments, energy balance, intermittency, microscales and integral scales. Using a new method of analysing hot-wire signals Rodi (1975*a*) made measurements of mean velocity and turbulent intensities and showed that the mean velocity decay along the axis of the jet conformed to the x^{-1} decay expected from similarity analysis, unlike the measurements of W & F. Seif (1981), analysing the data of both W & F and Rodi found a significant shortfall in the momentum flux across the jet. Capp (1983) and George *et al.* (1988) hypothesized that a return flow that might be set up in the entrainment regions of the jet facility may explain this lack of conservation of momentum and derived a criterion relating the volume flux of the jet and the room size to the expected momentum loss with distance. Capp (1983) and Hussein (1988) undertook laser-Doppler (LDA) measurements and stationary hot-wire (SHW) measurements in a round jet with nozzle exit conditions close to that of W & F but in a much larger room, to emulate a jet in an infinite environment. These measurements are reported in Capp, Hussein & George (1990, hereafter referred to as CHG with suffixes LDA and SHW to indicate the type of measurement system). Significant differences between the LDA and SHW measurements of CHG are observed, especially in higher-order moments. The differences were attributed to rectification, drop-out and cross-flow errors in stationary hot-wire anemometry, with LDA measurements considered more reliable. Note that Hussein (1988) also made flying hot-wire measurements of triple moments for his thesis, which closely matched the LDA measurements in the same facility. We compare only with the LDA measurements.

Models for triple moments for use in second-order closure of the Reynolds stress equations express triple moments in terms of second moments. Lumley (1978) and Dekeyser & Launder (1983) describe two approaches that are currently used. Basic models for triple moments give explicit representation in terms of second moments. More complicated models give an algebraically coupled formulation for triple moments. Taulbee (1988) and Taulbee, Hussein & Capp (1987) evaluated the performance of the basic triple moment models using the LDA data of CHG and found that the model profiles predicted the shapes well but underpredicted the values. The triple-moment models are considered in more detail in §4.3 where they are compared with measurements.

In the present study measurements were made in air and helium round jets of the same nozzle momentum efflux. In this paper measurements made in an air jet of diameter 6.1 mm at a Reynolds number of 1.1×10^4 are reported. The helium jet measurements are reported in a companion paper (Panchapakesan & Lumley 1993). Velocity moments in the air jet were obtained with ×-wire probes, moved through the jet with a shuttle. In §§2 and 3 we present details of the experimental set-up and the governing equations. In §4.1 measurements of mean velocity and higher moments are presented. Kinetic energy and component energy budgets and dissipation profiles are discussed in §4.2. Comparisons of triple-moment models with experimental data are presented in §4.3.

2. Experimental set-up, calibration and data reduction

The choice of initial conditions and the characterization of the jet flow from the nozzle are important. There are primarily two alternatives available – laminar flow or fully developed turbulent pipe flow at the nozzle exit. As emphasized by Gouldin *et al.* (1986), an initially laminar flow can be characterized completely but the transition of that flow to turbulence is difficult to calculate. Fully developed pipe

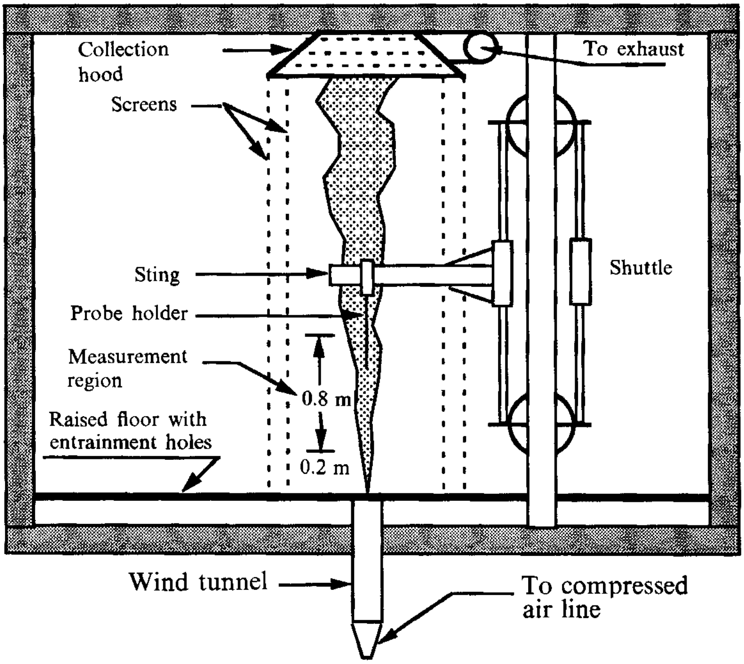

FIGURE 1. Sketch of the experimental set-up. Room size: 4.25 × 4.25 × 3.75 m.

flow is more attractive from a computational point of view but is difficult to characterize satisfactorily and consequently comparisons with other studies are difficult. Previous jet studies have mostly used an initially laminar flow. The present experimental set-up was designed to emulate a jet at the centre of an infinite flat plate with laminar flow of 'top-hat' velocity profile.

A large windowless room housed the experimental set-up as shown in figure 1. This minimized temperature variations and flow disturbances. A small wind tunnel of circular cross-section was used to produce the jet. The nominal diameter of the wind tunnel was 10 cm. The tunnel was mounted flush at the centre of a raised wooden floor, about 8 cm from the room floor. The raised wooden floor had a large number of holes (3.5 cm diameter) for the flow of entrainment air (the passage between the two floors was open on one side to supply the ambient air for entrainment). Two circular concentric screens (16 meshes per in.) spaced 6 cm apart were hung from a collection hood mounted on the ceiling. The diameter of the inner screen was 1 m. The entrainment holes were distributed only outside these screens. The collection hood at the top was connected to an exhaust blower with a throttle. The flow rate was adjusted to match the expected jet mass flux near the hood. The measurements were found to be relatively insensitive to the blower setting. The hood was at a distance of 450 diameters (2.8 m) from the nozzle while the measurements were confined to 30–150 diameters (0.2–1.0 m).

A laboratory compressed air supply metered with a needle valve was fed through a diffuser to the wind tunnel. A nozzle machined out of a cylindrical block of acrylic with a matched bi-cubic profile provided the jet. A large contraction ratio (≈ 267) minimized the boundary-layer thickness at nozzle exit. Consequently a top-hat velocity profile was assumed. This was verified with a traverse of a hot wire of very small length. Jet exit velocity was monitored with a pressure transducer and was maintained to within ±0.05% of the desired velocity. The turbulence intensity at the nozzle exit was of the order of 0.01%, a very low value made possible by the use of the compressed air supply.

The geometric axis of the jet and the run of the shuttle (see below) were carefully aligned to coincide with the vertical, and the axisymmetry of the jet was checked by measurement of mean velocity.

Measurements were made with a TSI 1241 × -probe and DISA 55M anemometers. The probe was mounted on a sting and moved through the jet from the top to the bottom with a shuttle. The shuttle velocity was set at around 2 m/s. The shuttle consisted of two carriages each sliding over two long rods on air bushings. The sting was attached to one carriage and counterweights to the other. The cantilever portion of the sting was also balanced. The two carriages were connected by taut cables running over two pulleys at the top and the bottom. The cyclic operation of the shuttle, controlled by an electronic timer circuit, consisted of the following phases: acceleration, free travel, braking, and return. The total cycle time was about 8 s: the downward travel of the sting was completed in about 1 s and the return and dwell in 7 s. The dwell was adjusted to be long enough for the disturbances induced by the sting motion to be washed away or dissipated. This was verified with measurements in quiescent air.

The speed of about 2 m/s for the shuttle traverse was chosen partly because, at this speed the oscillations associated with the initial kick die well before entering the measurement range. More important, however, this speed was found to be more than adequate to resolve the reverse flow. Plots of the traces of voltage signals as measured by the hot wires were superimposed on the calibration domain and were found to be well inside the domain, indicating that the reverse flows were being well resolved.

The shuttle was set in motion by kicking the counterweight carriage with a pair of air cylinders at the bottom and was braked and motion reversed at the top by another pair. These two phases each used 0.2 m of the total shuttle traverse of 2 m. An umbilical cord accommodated the movement of the probe cables, control signal cables and air supply to bushings.

The inherent noise in the flying wire system was extremely small (smaller than that of the calibration-inversion scheme; see below). This was checked by taking flying-wire measurements with the flow turned off. The variations seen in figure 4, for example, are due to an inadequate statistical sample. As indicated below, all averages were calculated using 1000 shuttle runs.

The ×-wire probe was calibrated in a calibration tunnel similar to the jet tunnel, but with a nozzle diameter of 15 mm. A full velocity–yaw angle calibration scheme was used. The calibration domain consisted of angle range of ±42° and velocity range of 0.8–12 m/s. The minimum velocity was determined by the choice of shuttle speed and the strength of flow reversals in the edge region of the jet. The maximum velocity was varied depending on the measurement location in the jet. Computer-controlled stepper motors were used to position the probe at N_{yaw} different angles Θ and to set the velocity U at N_{vel} velocities with the help of a pressure transducer. At each setting (U_s, Θ_s) a wire voltage pair (E_1, E_2) was recorded. Conversion of these voltages into (U_c, Θ_c) was done with a table-look-up scheme described by Lueptow, Breuer & Haritonidis (1988) with a few modifications to suit our needs:

(i) An initial transformation (essentially polar to rectangular), equivalent to

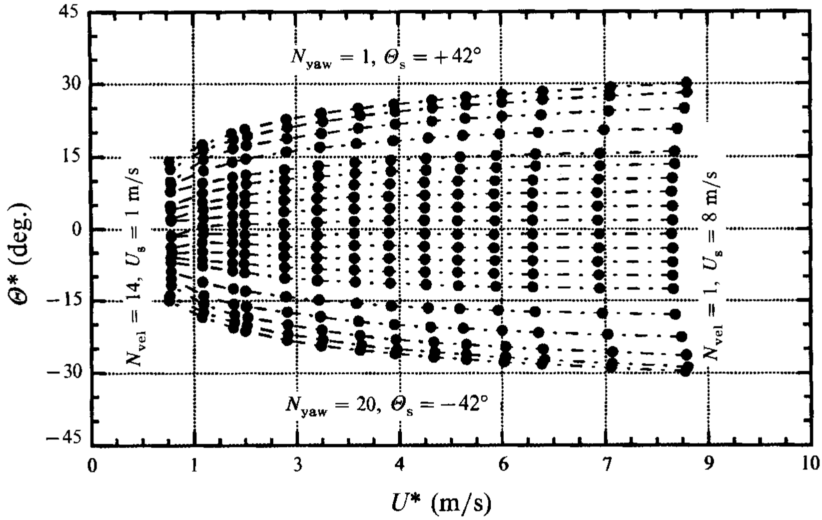

FIGURE 2. The calibration domain for the × -wire probe in the intermediate variables (U^*, Θ^*) (see (1)).

assuming King's law and the Cosine law, was applied to the voltage pair (E_1, E_2) to convert them to a pair of intermediate variables (U^*, Θ^*):

$$U_{i(\text{eff})} = \{(E_i^2 - a_i)/b_i\}^{1/n_i}, \tag{1a}$$

$$U^* = \{U^2_{1(\text{eff})} + U^2_{2(\text{eff})}\}^{0.5}, \tag{1b}$$

$$\Theta^* = 45 - \tan^{-1}\{U_{2(\text{eff})}/U_{1(\text{eff})}\}, \tag{1c}$$

where a_i, b_i and n_i are constants in the King's law representation of the hot-wire calibration with flow normal to the wires, and $U_{i(\text{eff})}$ are effective cooling velocities. This transformed the domain of calibration into a near rectangular region as shown in figure 2 and enabled more effective use of the look-up table arrays and also prevented loss of resolution in the low-velocity region.

(ii) For each of the N_{yaw} lines (indicated as dotted lines in figure 2) the variables U_s, Θ_s and Θ^* were curve fitted as functions of U^*.

(iii) For about 400 points between U^*_{min} and U^*_{max} the variables U_s, Θ_s and Θ^* were evaluated and the values of U_s and Θ_s were curved fitted as functions of Θ^* at each value of U^*. The coefficients of these fits were stored.

During measurement the following steps were used to calculate U and Θ from wire voltages:

(i) The voltage pair (E_1, E_2) was converted to (U^*, Θ^*);

(ii) U and Θ values were evaluated at Θ^* with curve fits at U_i^* and U_{i+1}^* flanking U^*;

(iii) U and Θ values at U^* were evaluated using linear interpolation.

The result of this inversion scheme operating on the calibration data is shown in figure 3. Figure 3(*a*) shows the calculated velocity U_c plotted against U_s for all angular positions and figure 3(*b*) shows a similar plot for Θ for all velocities. The r.m.s. errors in velocity and angle were about 1.0 cm/s and 0.5° respectively.

The full range of velocities encountered during the probe travel from the low-velocity region at the top (large-x/d locations) to the high-velocity region closer to

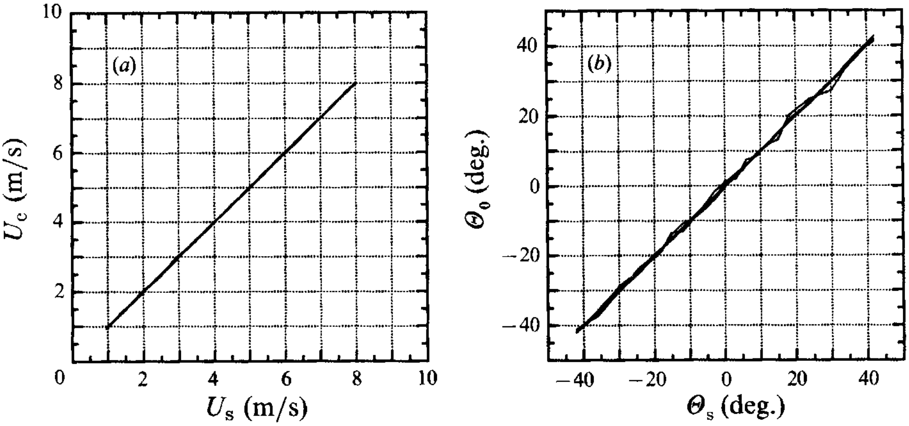

FIGURE 3. ×-wire calibration inversion. (*a*) The set velocity U_s plotted against the calculated velocity U_c for all angles shown in figure 2. (*b*) The set angle Θ_s plotted against Θ_c for all velocities shown in figure 2.

the nozzle necessitated the use of an offset amplifier between the anemometers and the A/D converter inputs. This amplifier subtracted a known constant voltage, measured with a high-precision voltmeter, from the anemometer outputs and amplified the signal sufficiently to span the A/D converter voltage range. The offset voltage was added to the digitized values in the processing software to reconstruct the anemometer voltages. Use of mercury batteries eliminated drift of offset voltages. The amplifier had a filter stage which was d.c. coupled and had a cutoff frequency of about 15 kHz.

The probe was positioned at different radial locations along the sting from the centreline to the edge of the jet. At each radial location the ×-wire probe was mounted in two different orientations to get u and v, and u and w components of velocity. A long strip of 16 mm film with sprocket holes fixed to the shuttle support column, and an infrared photoelectric cell mounted on the shuttle carriage, provided a timing signal which was used to measure the speed of the shuttle during the first half of the free travel and to digitize the probe voltages during the second half. The timing signal enabled digitization of probe voltages at the same spatial locations during each shuttle traverse in the x/d range from 30 to 150 with a spacing of 1.25 diameters. At each radial location, data for 1000 traverses were digitized and stored. Ensemble averages of all moments up to fourth order were calculated from these 1000 traverses. All statistical averages were curve fitted as functions of x/d using least-square b-splines. From these spline-fit representations the values at different x/d locations were calculated to obtain radial variations of the moments.

3. Governing equations

The jet is described using a cylindrical coordinate system with $x^i = (r, \theta, x)$ to indicate the radial, azimuthal and axial directions of the jet. The axial direction is vertical. The jet is axisymmetric and there is no swirl so that the azimuthal mean velocity and all correlations involving odd powers of the azimuthal component are zero. The components of the mean and fluctuating velocity fields are denoted by

$$U^i = U_i = (V, 0, U); \quad u_i = (v, rw, u); \quad u^i = (v, w/r, u). \tag{2}$$

The superscripts and subscripts indicate contravariant and covariant components, the symbols without subscripts indicate physical components. A comma in the subscript indicates covariant differentiation with respect to the index that follows and $\langle\ \rangle$ indicates averaging. Repeated indices imply summation.

The continuity and mean momentum equations in constant-density incompressible steady turbulent flows, in general tensor notation, are given by

$$U^i_{,i} = 0, \tag{3}$$

$$U^m U_{i,m} = -(1/\rho) P_{,i} - \langle u_i u^m \rangle_{,m} + \nu g^{km} U_{i,km}, \tag{4}$$

where g^{km} is the metric tensor and ν is the kinematic viscosity. P and p denote mean and fluctuating pressure fields. These equations are used in §4.1 to check the consistency of Reynolds stress measurements and conservation of momentum. The Reynolds stress equation is given by

$$U^m \langle u_i u_j \rangle_{,m} = P_{ij} + R_{ij} + T_{ij} - \epsilon_{ij}, \tag{5}$$

where

$$\begin{aligned}
P_{ij} &= -(\langle u_j u^m \rangle U_{i,m} + \langle u_i u^m \rangle U_{j,m}) && \text{(production)},\\
R_{ij} &= -(1/\rho)(\langle p_{,i} u_j \rangle + \langle p_{,j} u_i \rangle) && \text{(pressure effects)},\\
T_{ij} &= -(\langle u_i u_j u^m \rangle - \nu g^{km} \langle u_i u_j \rangle_{,k})_{,m} && \text{(transport)},\\
\epsilon_{ij} &= 2\nu g^{km} \langle u_{i,m} u_{j,k} \rangle && \text{(dissipation)}.
\end{aligned}$$

The equations for the budgets of component energies and the Reynolds stress $\langle uv \rangle$ can be derived from (5). We consider these budgets in §4.2. Second-order modelling describes turbulent flows with the Reynolds stress equation by providing models for the unknown terms: R_{ij}, T_{ij} and ϵ_{ij}. We will evaluate some of the current models for the triple-moment term in T_{ij} in §4.3. The models for triple moments are conveniently viewed as closures of the triple-moment equation:

$$U^m \langle u_i u_j u_k \rangle_{,m} = P^{(\mathrm{T})}_{ijk} + P^{(\mathrm{M})}_{ijk} + d_{ijk} + \phi_{ijk} - \epsilon_{ijk}, \tag{6}$$

where

$$\begin{aligned}
P^{(\mathrm{T})}_{ijk} &= [\langle u_j u_k \rangle \langle u^m u_i \rangle_{,m} + \langle u_k u_i \rangle \langle u^m u_j \rangle_{,m} + \langle u_i u_j \rangle \langle u^m u_k \rangle_{,m}]\\
&\quad \text{(turbulent production)},\\
P^{(\mathrm{M})}_{ijk} &= -[\langle u_j u_k u^m \rangle U_{i,m} + \langle u_k u_i u^m \rangle U_{j,m} + \langle u_i u_j u^m \rangle U_{k,m}]\\
&\quad \text{(mean-strain production)},\\
d_{ijk} &= -[\langle u_i u_j u_k u^m \rangle - \nu g^{nm} \langle (u_i u_j u_k) \rangle_{,n}]_{,m}\\
&\quad \text{(turbulent and viscous transport)},\\
\phi_{ijk} &= (1/\rho)[\langle p_{,i}(u_j u_k) \rangle + \langle p_{,j}(u_k u_i) \rangle + \langle p_{,k}(u_i u_j) \rangle]\\
&\quad \text{(pressure effects – dispersive and non-dispersive)},\\
\epsilon_{ijk} &= 2\nu g^{nm}[\langle u_i u_{j,n} u_{k,m} \rangle + \langle u_{i,n} u_j u_{k,m} \rangle + \langle u_{i,n} u_{j,m} u_k \rangle]\\
&\quad \text{(dissipation)}.
\end{aligned}$$

In free turbulent flows, away from walls, the viscous contributions to the transport terms in (4), (5) and (6) are negligible in comparison with the turbulent contributions and hence will be neglected.

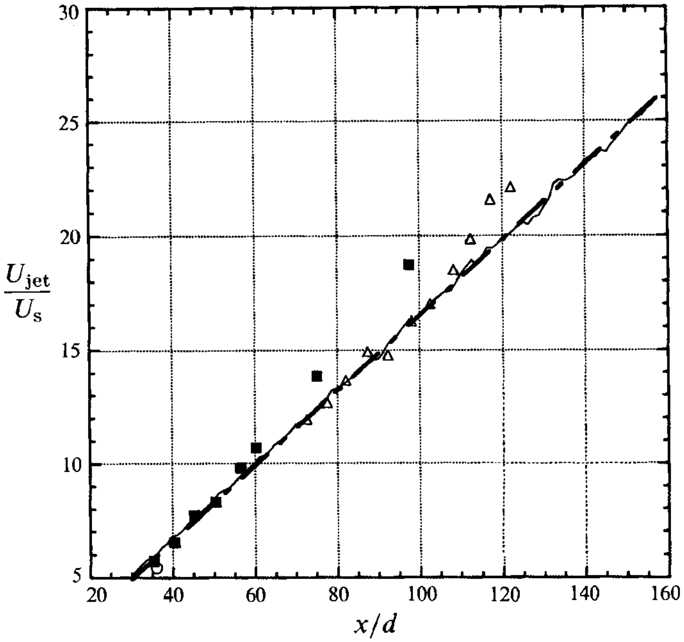

FIGURE 4. Variation of centreline mean velocity U_s along the jet axis: ——, U_{jet}/U_s; —·—·—, best linear fit to the data through the origin $x/d = 0$ given by $U_{\text{jet}}/U_s = 0.165 \times x/d$; ○, SHW-CHG – Stationary Hot-Wire measurements of Capp *et al.* (1990); △, LDA-CHG – LDA measurements of Capp *et al.* (1990); ■, W & F – Wygnanski & Fiedler (1969).

	W & F	Rodi	SHW-CHG	LDA-CHG	Present
Reynolds number	$\sim 10^5$	8.7×10^4	$\sim 10^5$	$\sim 10^5$	1.1×10^4
Jet velocity	51 m/s	101 m/s	56 m/s	56 m/s	27 m/s
Jet diameter	25.4 mm	12.0 mm	25.4 mm	25.4 mm	6.1 mm
Method	SHW	SHW	SHW	LDA	Shuttle-mounted hot wire
Mean velocity decay constant	5.4	5.9	5.9	5.8	6.06
Spreading rate	0.086	0.086	0.102	0.094	0.096

TABLE 1. Experimental conditions and some mean flow parameters: a comparison between the present results and those of Wygnanski & Fiedler (1969), Rodi (1975*a*) and Capp *et al.* (1990)

4. Results

4.1. *Mean velocity and second moments*

Measurements of mean velocity and turbulent intensities in turbulent round jets with top hat velocity profiles at the nozzle exit have been reported by many authors. There are however significant differences between different studies. We compare our results primarily with those of W & F, Rodi, SHW-CHG and LDA-CHG. Details of experimental conditions along with some mean flow parameters are given in table 1.

The axial variation of axial mean velocity is shown in figure 4. For the range $x/d = 30$ to 160 we see no deviation from the x^{-1} decay ($U_{\text{jet}}/U_s = 0.165x/d$). Capp (1983) and CHG argue that the deviation from the inverse-law decay such as that

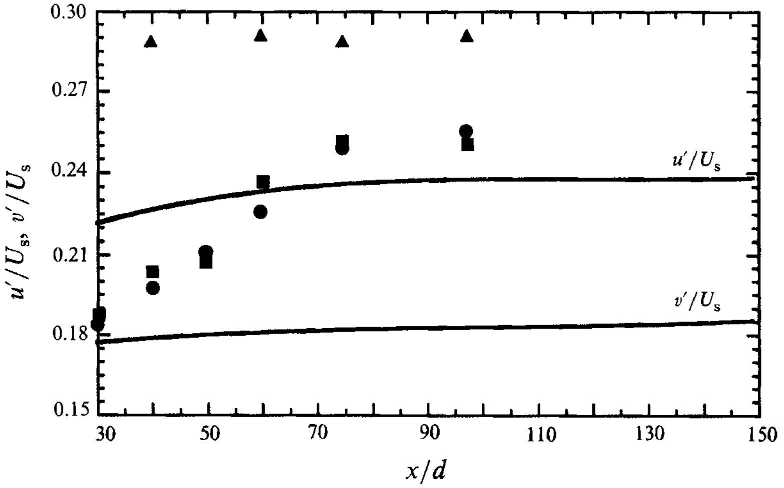

FIGURE 5. Variation of turbulent intensities u'/U_s and v'/U_s along the jet centreline. Present measurements: ——, u'/U_s and v'/U_s. W & F: ▲, u'/U_s; ●, v'/U_s; ■, w'/U_s.

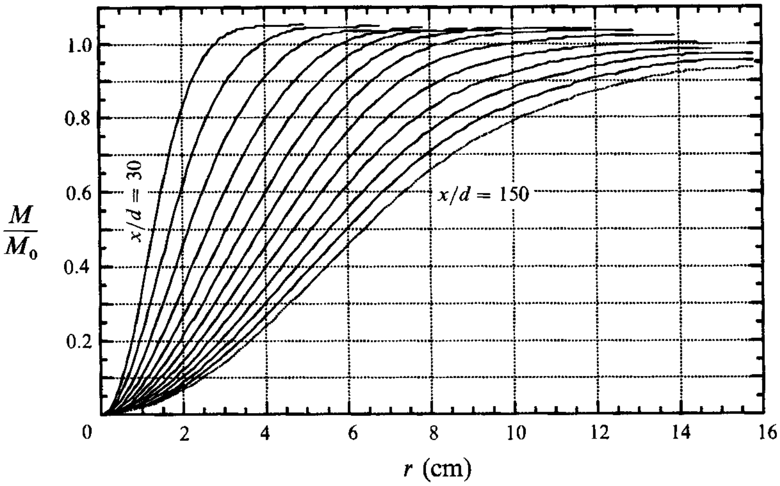

FIGURE 6. Ratio of integrated momentum flux across the jet $M(r)$ to the nozzle input M_0 at various axial locations. (Note: $M\infty$) corresponds to M in (7).)

found in the measurements of W & F may have been due to effects of confinement of the jet and give an analysis for the expected momentum loss due to reverse flow set up by the confinement. The low volume flux of our jet and the size of the room ensure that thre would be only 0.5 % loss in momentum flux at $x/d = 150$ according to the above analysis even if the jet flow was not exhausted. The axial variations of turbulent intensities are shown in figure 5. The axial component reaches its self-similar value at about $70x/d$ while the radial component seems to increase very slowly throughout.

The mean axial momentum equation can be integrated over the cross-section of the jet to relate the momentum flux across the jet, M, to the momentum efflux at the nozzle, M_0:

$$M = 2\pi\rho \int_0^\infty [U^2 + u^2 - \tfrac{1}{2}(v^2 + w^2)]\, r\, \mathrm{d}r = M_0, \tag{7}$$

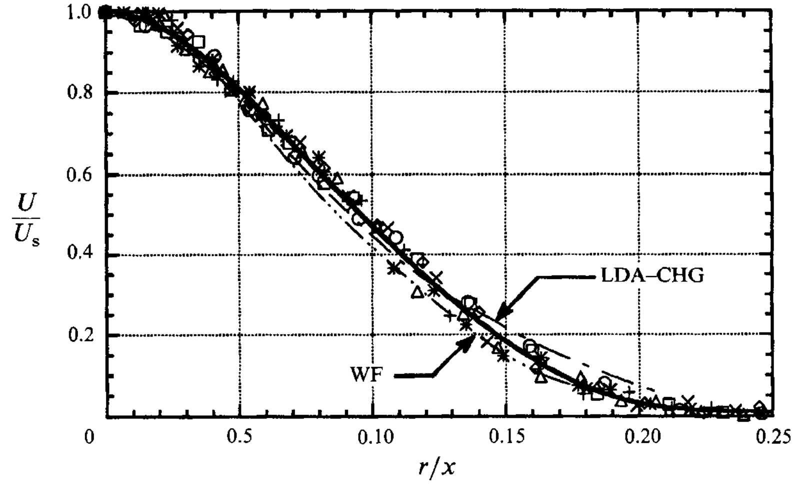

FIGURE 7. Axial mean velocity profile across the jet. +, $s/d = 60$; *, 70; ○, 80; △, 90; ×, 100; □, 110; ◇, 120; ——, least-squares spline fit through the entire data set; WF, Wygnanski & Fiedler (1969); LDA-CHG, LDA measurements of Capp *et al.* 1990.

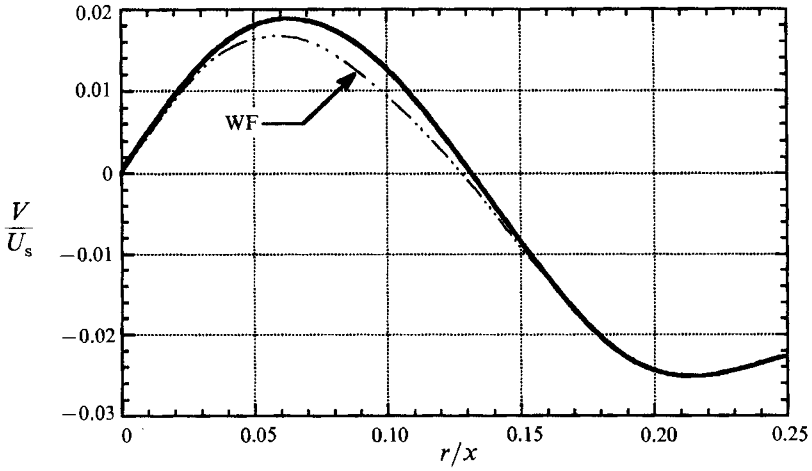

FIGURE 8. Radial mean velocity obtained from the curve fit of figure 7 and the continuity equation.

where the pressure gradient has been evaluated using the cross-stream momentum equation and the viscous terms have been ignored (see Tennekes & Lumley 1972). This integral has been evaluated directly from measurements at various x/d values from 30 to 150, figure 6, and the ratio M/M_0 is within $\pm 5\%$ of unity, indicating that the measurements are consistent with the equations of motion. CHG also report a similar agreement: 0.97 for LDA measurements and 1.07 for SHW measurements at $x/d = 70$. Seif (1981) estimated that the data of W & F and Rodi account only for 0.60 and 0.84, respectively, of the nozzle input in the self-similar region. Variation of the axial mean velocity in the radial direction is shown in figure 7, where U_s, the scale velocity, is the centreline mean velocity. The profile is very close to the LDA measurements of CHG although there is some divergence near the edge of the jet. The half-width for the mean velocity profile, the value of r/x when $U/U_s = 0.5$, was 0.096. The half-width of the jet can be used to determine the representation of the mean

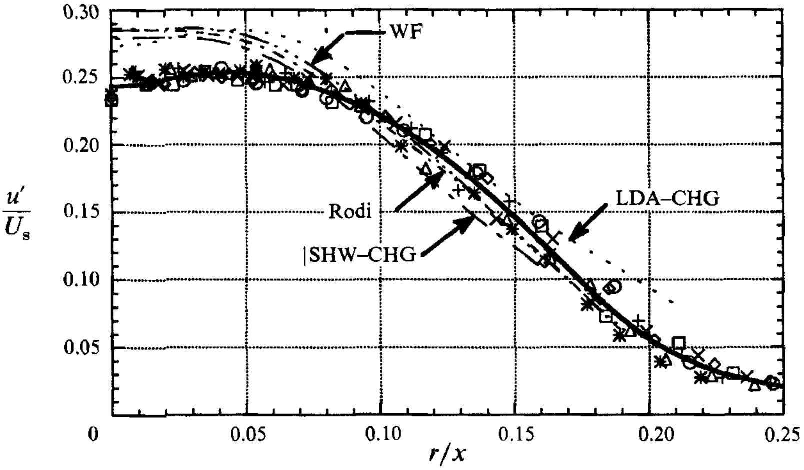

FIGURE 9. Turbulence intensity of the axial velocity fluctuations across the jet: SHW-CHG, stationary hot-wire measurements of Capp *et al.* (1990); Rodi, Rodi (1975*a*). Other symbols are the same as in figure 7.

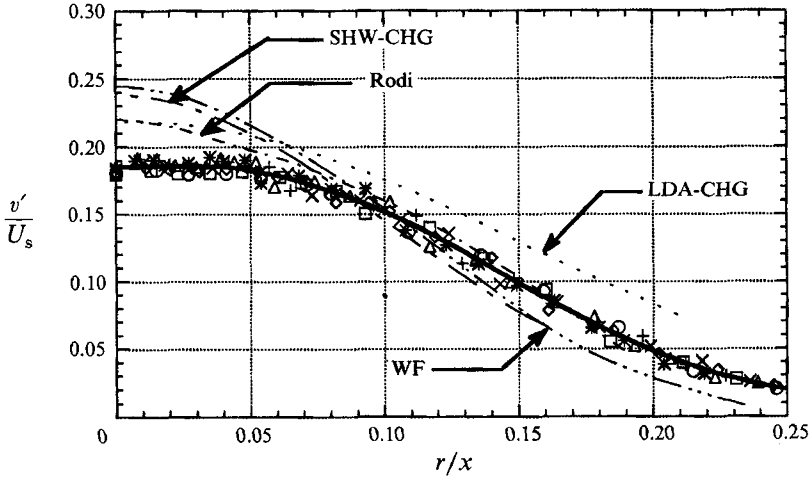

FIGURE 10. Turbulence intensity of the radial velocity fluctuations across the jet. See figures 7 and 9 for explanation of symbols.

velocity profile in the form $U/U_s = \exp(-K_u \eta^2)$. This gives a value of $K_u = 75.2$. Integration of the mean velocity profile using this representation gives the ratio of mass flux at a section to the mass flux at the nozzle to be $m/m_0 = 0.32x/d$. This is in agreement with the direct measurement of entrainment by Ricou & Spalding (1961) who give the same relation for an air jet but indicate that this constant of proportionality is independent of Reynolds number only beyond 2.5×10^4 and that the entrainment rate is slightly higher at lower Reynolds numbers. The radial mean velocity calculated from the axial mean velocity profile using the continuity equation is shown in figure 8.

The radial profiles of turbulent intensities and Reynolds stress $\langle uv \rangle$ are shown in figures 9–12. There is an off-axis peak in the profile of the axial velocity fluctuations which is also seen in the LDA measurements. This is not clearly observed in other measurements in the far field, but has always been seen in the near field, close to the

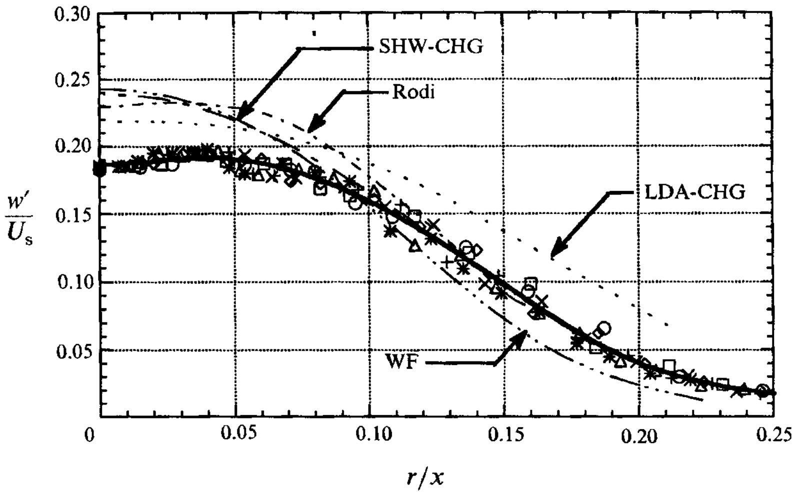

FIGURE 11. Turbulence intensity of the azimuthal velocity fluctuations across the jet. See figures 7 and 9 for explanation of symbols.

nozzle. This peak is expected from the profile of shear production of kinetic energy which has a distinct off-axis peak at nearly the same location. The profiles for the turbulent intensities are lower than other hot-wire measurements in the central core of the jet but are higher in the outer region. The LDA measurements of CHG are significantly higher than the present measurements in the outer region of the jet. The higher values of the present measurements in comparison with other hot-wire measurements in the outer region are expected because the bias velocity of the shuttle eliminates rectification and drop-out errors associated with stationary hot-wire measurements. The turbulent intensity of axial velocity fluctuations based on local mean velocity as seen by the probe on the shuttle was less than 18% at $x/d = 60$ and less than 12% at $x/d = 120$ at all radial locations. This keeps the instantaneous velocity vector well within the angle of acceptance of the probe. It must be emphasized that for stationary hot-wire probes the turbulence intensity based on local mean velocity is well above 100% in the edge region of the jet and the instantaneous velocity vector may lie outside the probe acceptance angle with a high probability, leading to drop-out errors. The errors associated with the velocity component perpendicular to the plane of the × -wire are still present, but should be smaller than for stationary hot-wire measurements because of the lower apparent turbulence intensity seen by the probe. The intensities of all three velocity components on the axis of the jet are considerably lower in the present measurements – 24% for u' and 18.5% for v' and w' in comparison with 27–29% for u' and 22–25% for v' and w'. Browne, Antonia & Chua (1989), who also used a full velocity–yaw angle calibration scheme, report measurements in a jet of Reynolds number 17770, a value closer to the preent measurements. At $x/d = 15$ they find the turbulence intensities of u and v on the axis to be about 21.3% and 16%. These values compare very well with our measurements of 22% and 17.5% for u' and v' at $x/d = 30$.

The Reynolds stress profile is shown in figure 12 along with the values estimated from the mean momentum equation with the following formula:

$$\frac{\langle uv\rangle}{U_s^2} = \frac{1}{\eta}\frac{U}{U_s}\int_0^{\eta}\frac{U}{U_s}\eta^*\,\mathrm{d}\eta^* + \eta\left(\frac{\langle u^2\rangle}{U_s^2} - \frac{\langle v^2\rangle}{U_s^2}\right), \tag{8}$$

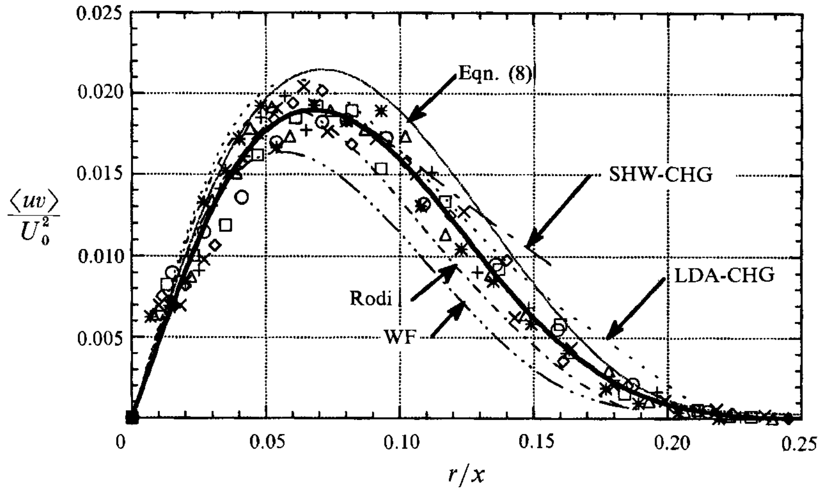

FIGURE 12. Reynolds stress variation across the jet along with the estimate from the mean momentum equation (8). See figures 7 and 9 for explanation of symbols.

where $\eta = r/x$. The estimate from the mean momentum equation is higher than curve-fitted values from measurements all across the jet but is close to the outer envelope of measured data points. Reynolds stress profiles from W & F and Rodi measurements are narrower than our present measurements and the LDA measurements of CHG, again a reflection of the resolution of flow reversals by the shuttle-mounted probe and LDA.

Gradients of third moments determine turbulent diffusion of turbulent kinetic energy and hence are important in estimating the kinetic energy budget. All non-zero third moments except $\langle vw^2 \rangle$ were measured. The profiles of measured third moments are shown in figure 13 along with the stationary hot-wire measurements of CHG and W & F and LDA measurements of CHG. In the region $0 < \eta < 0.04$ the correlations $\langle u^2v \rangle$, $\langle uv^2 \rangle$ and $\langle uw^2 \rangle$ were found to be negative, a feature also displayed by the LDA measurements but absent in the SHW measurements of CHG and W & F. These negative regions, especially that of $\langle u^2v \rangle$ which is responsible for the radial flux of the axial component of kinetic energy, considerably alter the picture of turbulent transport in the jet. The LDA measurements agreed very well with the present measurements near the axis and near the outer edge of the jet but were in general higher in the middle. The SHW measurements of CHG and W & F were found to agree both in shape and magnitude. The profiles for moments $\langle u^2v \rangle$ and $\langle v^3 \rangle$, involving odd powers of the radial fluctuating velocity, were wider in the present measurements than the SHW measurements, a possible consequence of the elimination of rectification and drop-out errors in the edge region. It was found that the levels of moments involving the radial component were sensitive to the accuracy of resolution of the angular dependence of the hot-wire calibration.

There are systematic differences between our measurements and those of other authors; the measurements of the other authors differ among themselves, even when measured by the same techniques. We certainly do not expect our measurements or LDA measurements to agree with the SHW measurements in the outer parts of the jet, but how can we explain the disagreements among all these measurements near the axis, where flow reversal is not a problem? Recall that we have evidence that our shuttle *was* moving fast enough to resolve reversals. All of these jets had nominally

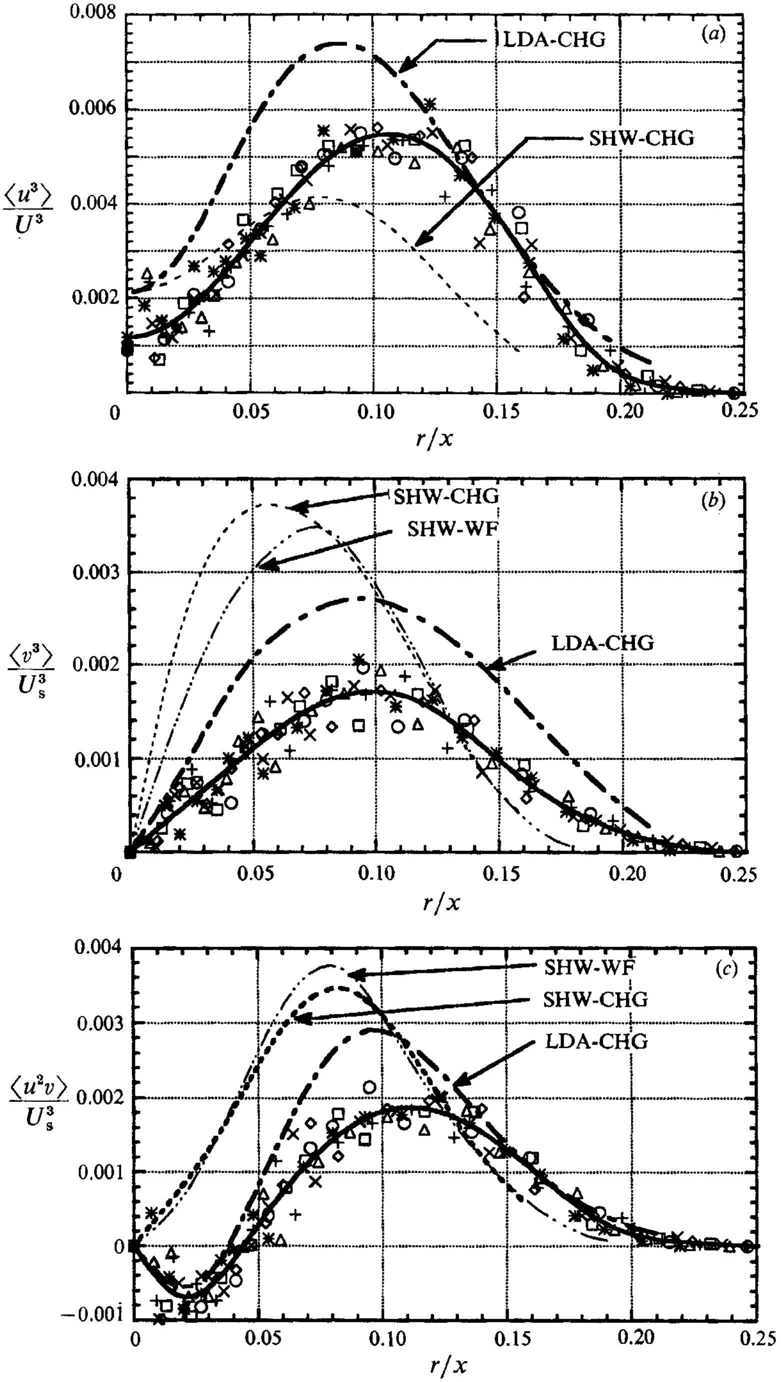

FIGURE 13(*a–c*). For caption see facing page.

top-hat nozzle exit velocity profiles with very low turbulence intensities. The Reynolds number of the present study was an order of magnitude lower than those of the other studies, and that is a possible explanation. Wygnanski has suggested (Wygnanski & Fiedler 1969) that the earlier measurements were made with

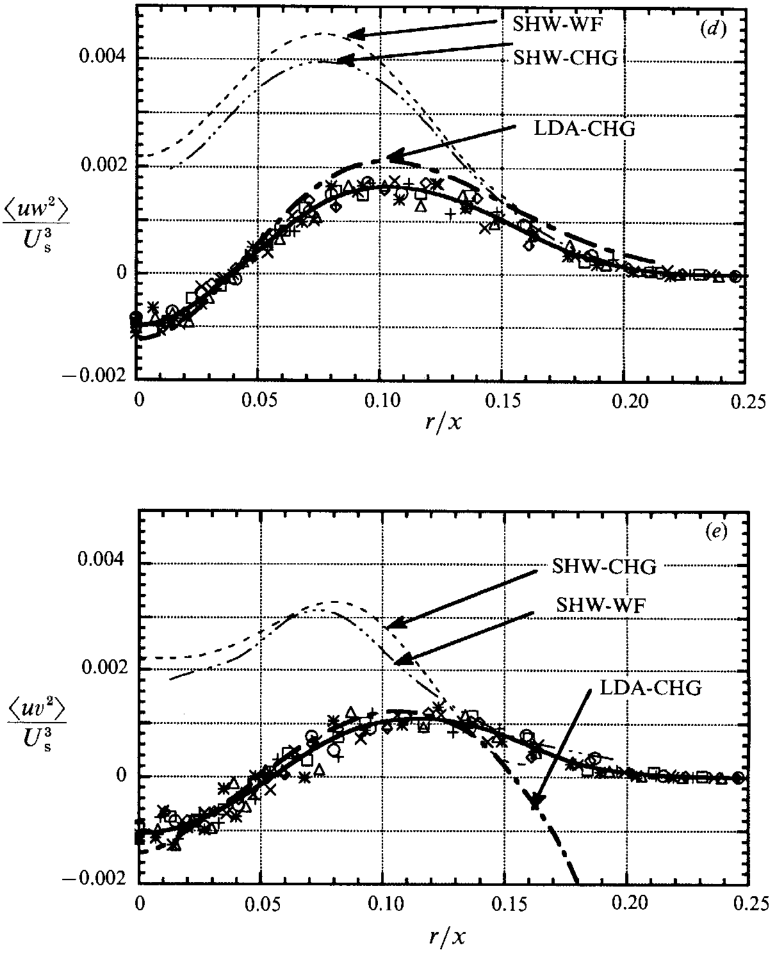

FIGURE 13. Variation of third moments across the jet normalized by U_s^3. (a) $\langle u^3 \rangle$, (b) $\langle v^3 \rangle$, (c) $\langle u^2 v \rangle$, (d) $\langle uv^2 \rangle$, (e) $\langle uw^2 \rangle$. See figures 7 and 9 for explanation of symbols.

capacitor-coupled circuits, and hence passed varying amounts of low-frequency large-scale motions. There are indications that all jet flows have more low-frequency large-scale motions than the best models (Duncan *et al.* 1992). This suggests that an axisymmetric jet is subject to a (probably helical) instability which is present to a greater or lesser extent in various experimental realizations; the flapping of the jet from side to side that results will affect the intensities near the axis by adding to them a more-or-less Gaussian part, and will have more complicated effects on the higher moments near the axis. This may explain the sign changes observed in some third-moment measurements by LDA and shuttle, but not by SHW. A more systematic study than the present one will be required to attribute the differences among these measurements to experimental technique or to any of these physical effects.

4.2. *Kinetic energy budget*

The equation for the kinetic energy is derived from the Reynolds stress equation (5), which for the axisymmetric jet, neglecting pressure and viscous diffusion, is

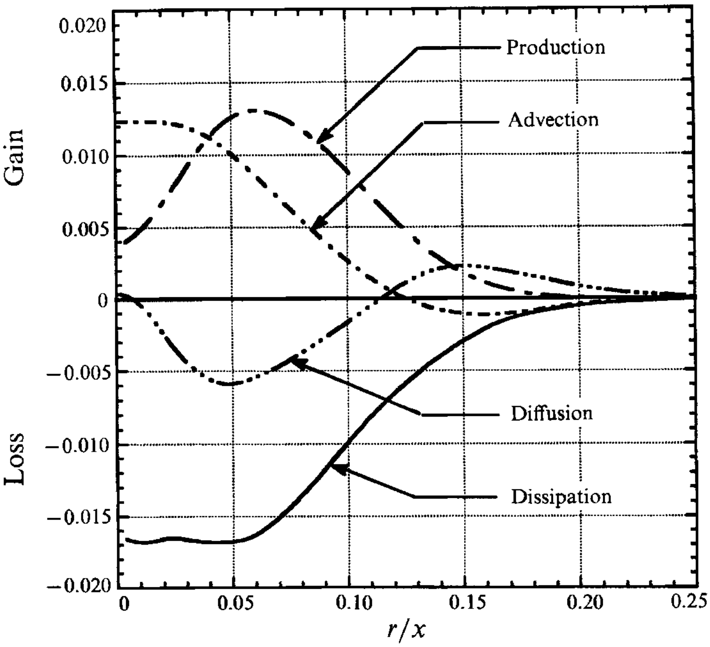

FIGURE 14. Kinetic energy budget for air jet based on equation (9). The curves have been normalized by U_s^3/L_u.

$$-\underbrace{\frac{1}{2}\left(V\frac{\partial\langle q^2\rangle}{\partial r}+U\frac{\partial\langle q^2\rangle}{\partial x}\right)}_{\text{advection}}-\underbrace{\left(\langle v^2\rangle\frac{\partial V}{\partial r}+\langle w^2\rangle\frac{V}{r}+\langle u^2\rangle\frac{\partial U}{\partial x}+\langle uv\rangle\left(\frac{\partial V}{\partial x}+\frac{\partial U}{\partial r}\right)\right)}_{\text{production}}$$

$$-\underbrace{\frac{1}{2}\left(\frac{\partial\langle q^2v\rangle}{\partial r}+\frac{\langle q^2v\rangle}{r}+\frac{\partial\langle q^2u\rangle}{\partial x}\right)}_{\text{diffusion}}-\underbrace{\epsilon}_{\text{dissipation}}=0, \tag{9}$$

where $q^2 = u_i u^i$. The kinetic energy budget is shown in figure 14, where the terms have been normalized using the factor L_u/U_s^3. L_u is the local lengthscale, taken to be the half-width of the jet, $L_u = r_{\frac{1}{2}}x$, where $r_{\frac{1}{2}}$, the non-dimensional half-width, is the value of η at which U/U_s is 0.5. For the present measurements $r_{\frac{1}{2}}$ is 0.096. The axial and radial derivatives of various quantities have been calculated from the self-similar profiles as follows:

$$Q^m = U_s^m f(\eta); \quad f' = \frac{\mathrm{d}f}{\mathrm{d}\eta}; \quad \frac{L_u}{U_s^m}\frac{\partial Q^m}{\partial r} = r_{\frac{1}{2}}f'; \quad \frac{L_u}{U_s^m}\frac{\partial Q^m}{\partial x} = -r_{\frac{1}{2}}(mf+\eta f'); \tag{10}$$

where Q^m is any turbulence moment of order m and $f(\eta)$ is its self-similar profile. The present budget differs from the budget presented by W & F. The production term is very similar to that of W & F but the advection term has a value of 0.0122 on the centreline and is comparable to the value of dissipation, while W & F found advection to be twice as large as dissipation on the centreline. The value of the advection term on the centreline is $r_{\frac{1}{2}}(\langle q^2\rangle/U_s^2)$ and hence the difference is due to the different measured values of $\langle q^2\rangle$. In calculating the diffusion term, the moment $\langle vw^2\rangle$, which was not measured, has been taken to be equal to $\langle v^3\rangle$. The diffusion profile, as expected, is very different from that of W & F. It is close to zero on the centreline

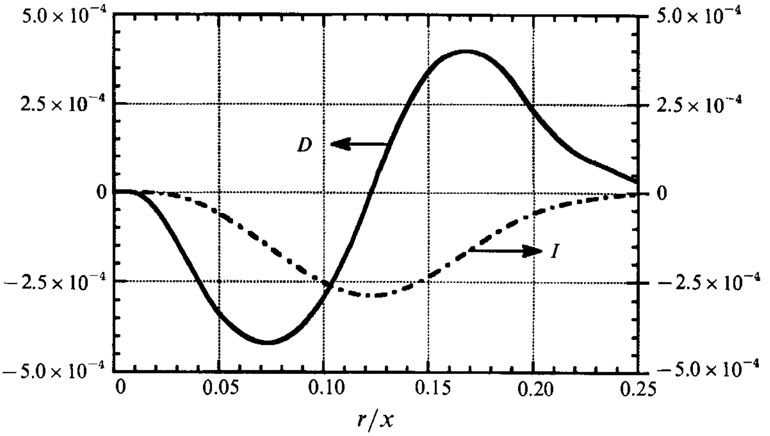

FIGURE 15. Plot of the radial diffusion of kinetic energy and its integral: $D = \eta(L_u/U_s^3)(1/r)\,\partial(r\langle q^2v\rangle/2)/\partial r$. I is the running integral of D.

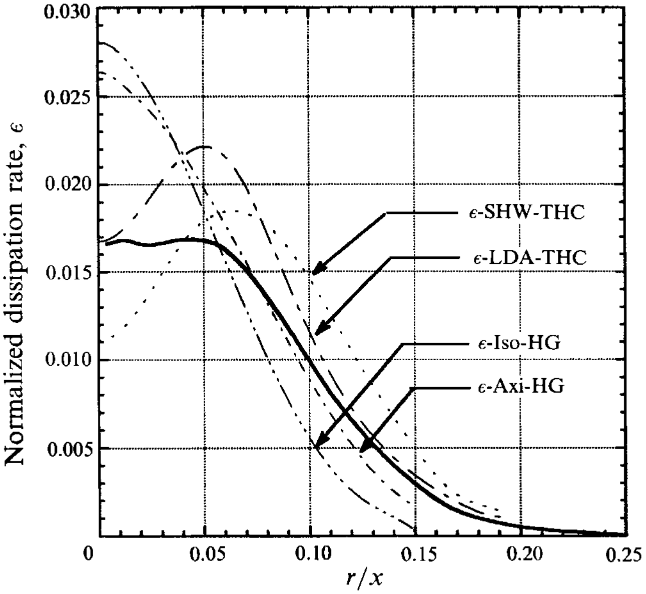

FIGURE 16. Comparison of profiles of the normalized dissipation rate $(L_u/U_s^3)\,\epsilon$ across the jet. ϵ-axi-*HG* and ϵ-iso-*HG* are estimates from direct derivative measurements assuming axisymmetry and isotropy of small scales reported in Hussein & George (1990). ϵ-SHW-THC and ϵ-LDA-THC are estimates from the budgets based on stationary hot-wire and LDA measurements reported in Taulbee *et al.* (1987). ——, Estimate from present measurements (see figure 14).

with a peak of about -0.006 at $\eta = 0.05$ and changes sign at $\eta = 0.115$. It is never as large as dissipation as was found by W & F. The radial diffusive flux of $\langle u^2\rangle$, given by $(1/r)(\partial(r\langle u^2v\rangle)/\partial r)$, is positive near the axis of the jet due to the negative slope of $\langle u^2v\rangle$. This gain is roughly balanced by the losses in $\langle v^2\rangle$ and $\langle w^2\rangle$, giving a net diffusive flux of $\langle q^2\rangle$ close to zero near the axis. The integral across the jet of the radial diffusive flux of kinetic energy should be zero as seen in figure 15.

The normalized dissipation profile, obtained from the budget as a balance, is compared with other measurements in figure 16. Hussein & George (1990) report

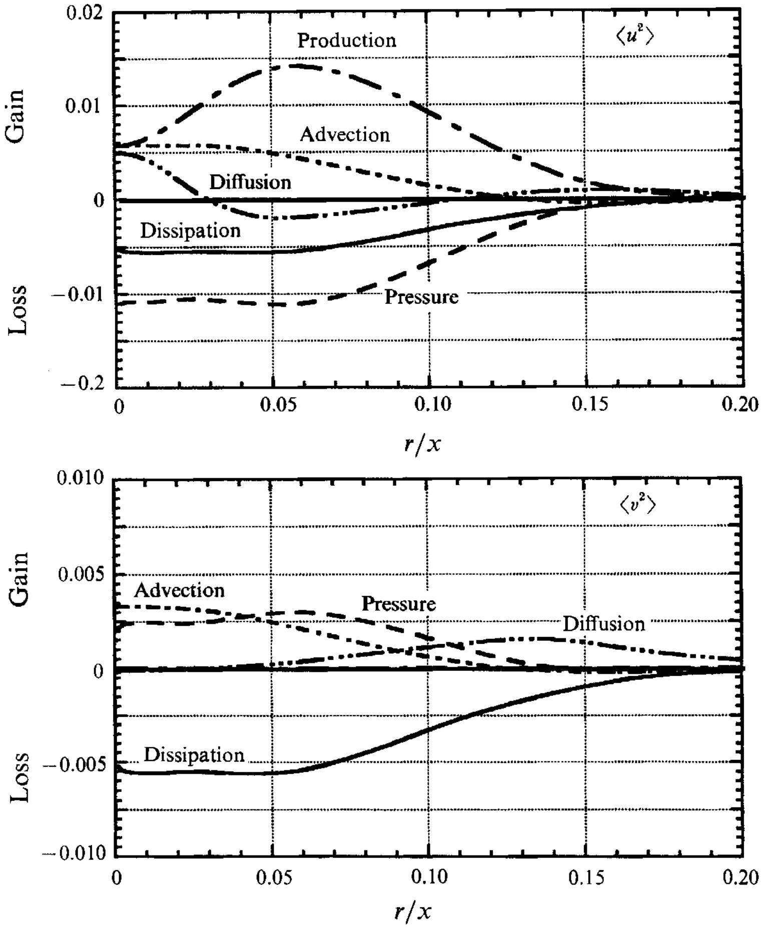

FIGURE 17. For caption see facing page.

estimates of dissipation from direct measurements of derivatives assuming isotropy and axisymmetry of small scales. These measurements were made in the same set-up used by CHG using a whirling arm to move hot-wire probes. The derivative measurements have been converted to normalized dissipation profiles using reported values of scale velocity, lengthscale and viscosity. Profiles from budgets of LDA and SHW measurements of CHG, reported in Taulbee *et al.* (1987), which take pressure diffusion into account using the model $(1/\rho)\langle pu_i\rangle = -0.2\langle q^2u_i\rangle$, are also shown. The present measurement does not show any off-axis peak as observed in the budgets reported by Taulbee *et al.* (1987) but has a rather flat region near the centre of the jet. Away from the core of the jet agreement with LDA measurements and direct measurements assuming axisymmetry is very good.

The component energy budgets and shear stress budget are shown in figure 17. The dissipation terms in these budgets have been obtained assuming small-scale isotropy, i.e. $\epsilon_{ij} = \frac{2}{3}\epsilon\delta_{ij}$ and we must bear in mind that the pressure diffusion term has been neglected in the estimation of ϵ. The pressure terms in the component energy budgets which contain both dispersive and non-dispersive effects have been obtained as the balance. The component energy budgets confirm the following well-known facts:

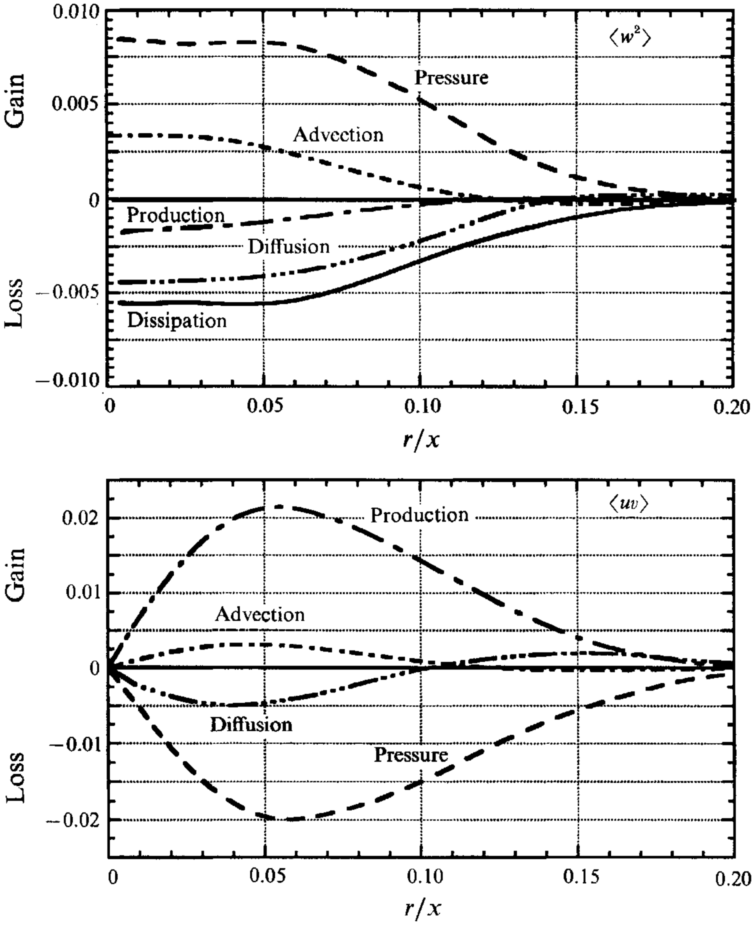

FIGURE 17. Budgets for component energies $\frac{1}{2}\langle u^2\rangle$, $\frac{1}{2}\langle v^2\rangle$, $\frac{1}{2}\langle w^2\rangle$ and Reynolds stress $\langle uv\rangle$.

(i) The energy production is almost completely in $\langle u^2\rangle$ and is predominantly shear production except near the axis where it is due to normal stress production.

(ii) The energy produced in $\langle u^2\rangle$ is transferred to $\langle v^2\rangle$ and $\langle w^2\rangle$ by the pressure redistribution term, and this redistribution is unequal with $\langle w^2\rangle$ receiving more than $\langle v^2\rangle$. From a balance point of view this comes about as a consequence of the behaviour of diffusion terms which is discussed below.

(iii) The advection terms have the same shape, with the centreline values proportional to the component energies.

The diffusion terms for each of the components can be written as

$$\left.\begin{array}{ll} u^2: & \dfrac{1}{r}\dfrac{\partial}{\partial r}(r\langle u^2v\rangle)+\dfrac{\partial}{\partial x}\langle u^3\rangle, \\[2ex] v^2: & \dfrac{1}{r}\dfrac{\partial}{\partial r}(r\langle v^3\rangle)+\dfrac{\partial}{\partial x}\langle uv^2\rangle-\dfrac{2\langle vw^2\rangle}{r}, \\[2ex] w^2: & \dfrac{1}{r}\dfrac{\partial}{\partial r}(r\langle vw^2\rangle)+\dfrac{\partial}{\partial x}\langle uw^2\rangle+\dfrac{2\langle vw^2\rangle}{r}. \end{array}\right\} \qquad (11)$$

The first term is the radial flux and the second term is the axial flux. The axial fluxes of v^2 and w^2 are negligible while that of u^2 is about 15% at its maximum in comparison with the radial fluxes. The third term in the v^2 and w^2 equations arises as a consequence of the change of elemental volume with radius and serves to interchange energy between v^2 and w^2 without changing the total kinetic energy. Near the axis of the jet the variations of the moments $\langle v^3\rangle$ and $\langle vw^2\rangle$ are almost linear, and assuming approximate equality of these moments it can be seen that the first and third terms are nearly equal in magnitude in that region. Consequently the diffusive flux of v^2 is almost zero near the axis while that of w^2 is twice the radial flux.

The shear stress budget is shown in figure 17 (*d*). The details of this budget are the same as the one presented by Rodi (1975*b*) for the measurement of W & F except for the magnitude of the production term and hence the pressure term. The peak value of production for the present measurements is 0.022 while that estimated by Rodi for W & F is about 0.028.

4.3. *Triple-moment models – evaluation*

In the Reynolds stress equations, the transport of the stresses by the fluctuating velocity field is given by the term $\langle u_i u^j u^k\rangle_{,k}$. Second-order modelling closes the Reynolds stress equations by expressing unknown correlations, such as this transport term, as a function of second moments. The model for triple moments proposed by Lumley (1978) is arrived at in the following manner: (i) The equation for the moment-generating function of velocity is modelled by requiring that turbulence relax to a Gaussian state in the absence of disturbing agencies such as inhomogeneity, buoyancy etc. and that it be consistent with the models used for second moments in the case of homogeneous turbulence. (ii) Neglect substantial derivatives and terms involving mean gradients by assuming that the turbulence is fine-grained (i.e. the lengthscale of turbulence is small compared to the lengthscale of inhomogeneity). If the resulting modelled equation for triple moments is viewed as a closure of the exact triple-moment equation (6) then the following models can be identified with individual terms:

$$\phi_{ijk} = \phi^{(1)}_{ijk} + \phi^{(2)}_{ijk}, \tag{12a}$$

$$\phi^{(2)}_{ijk} = -(3\beta/T)\left(\langle u_i u_j u_k\rangle - \tfrac{1}{9}[g_{ij}\langle q^2 u_k\rangle + g_{ik}\langle q^2 u_j\rangle + g_{jk}\langle q^2 u_i\rangle]\right), \tag{12b}$$

$$d_{ijk} = -[\langle u_i u_j\rangle\langle u_k u^m\rangle + \langle u_j u_k\rangle\langle u_i u^m\rangle + \langle u_k u_i\rangle\langle u_j u^m\rangle]_{,m}, \tag{12c}$$

$$\epsilon_{ijk} = (2/3T)[g_{ij}\langle q^2 u_k\rangle + g_{ik}\langle q^2 u_j\rangle + g_{jk}\langle q^2 u_i\rangle], \tag{12d}$$

where β is the return-to-istropy coefficient and is given by

$$\beta = 2 + \exp\left(-\frac{D}{R_1^{\frac{1}{2}}}\right)\left[\frac{72}{R_1^{\frac{1}{2}}} + A\ln\left(1 + B(-\mathrm{II} + C\mathrm{III})\right)\right]F, \tag{12e}$$

$$\mathrm{II} = -\tfrac{1}{2}b_i^j b_j^i, \quad \mathrm{III} = \tfrac{1}{3}b_i^j b_j^k b_k^i, \quad F = [\tfrac{1}{9} + 3\mathrm{III} + 2\mathrm{II}], \tag{12f}$$

$$b_i^j = (\langle u_i u^j\rangle/\langle q^2\rangle - \tfrac{1}{3}g_i^j, \tag{12g}$$

$$A = 80.1, \quad B = 62.4, \quad C = 2.3, \quad D = 7.77, \tag{12h}$$

$$T = \langle q^2\rangle/\langle\epsilon\rangle. \tag{12i}$$

The correlation with pressure ϕ_{ijk} is normally divided into two parts: $\phi^{(1)}_{ijk}$ is called the rapid part and $\phi^{(2)}_{ijk}$ is called the return-to-isotropy part. This division is suggested by the solution of the Poisson equation for the fluctuating pressure field which contains two terms: one that is quadratic in the fluctuating velocity field and is responsible for the return to isotropy of anisotropic homogeneous turbulence, the other is linear

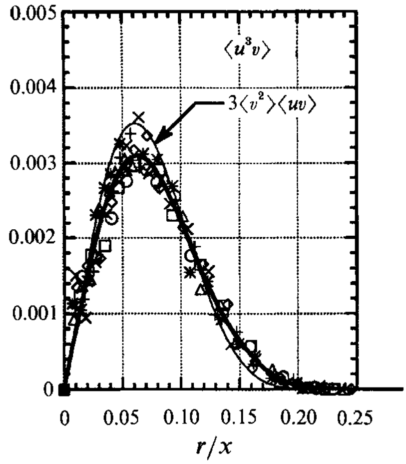

FIGURE 18. Variation of the fourth moments $\langle u^3v\rangle$ and $\langle u^2w^2\rangle$ across the jet and their quasi-Gaussian approximation according to (17). All values have been normalized by U_s^4.

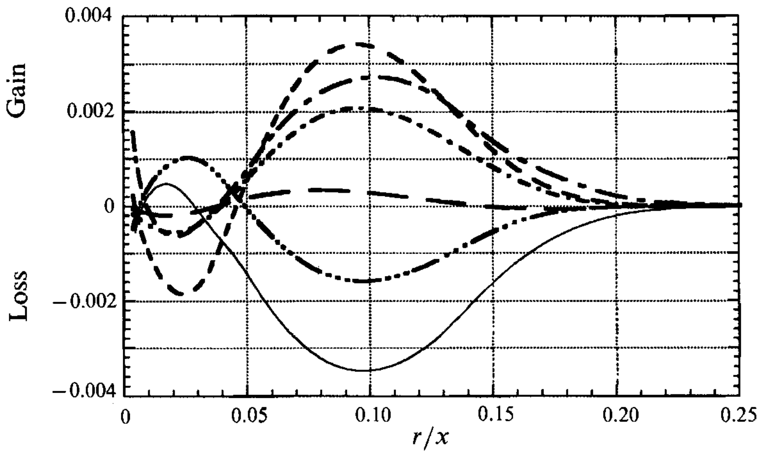

FIGURE 19. Budget for the triple moment $\langle u^2v\rangle$ based on (6): ——, advection; —···—, turbulent production; —·—·—, mean strain production; ———, diffusion; ---, estimate of the diffusion term with the quasi-Gaussian approximation; ——, estimate for the sum of pressure and dissipation terms obtained as the balance. all terms have been normalized by U_s^4/L_u.

in the fluctuating velocity field and mean velocity gradient and responds immediately to applied mean strain fields. The only undetermined constant in the model, the return-to-isotropy coefficient β, does not arise from the triple-moment modelling but appears as a consequence of the requirement of consistency with models for second-order quantities and its form is obtained by calibration against experiments on the return to isotropy of homogeneous anisotropic turbulence. The model for the triple moment, which shall be called the *Basic* model, is obtained by neglecting advection, mean-strain production and the rapid part of the pressure correlation in equation (6):

$$P^{(t)}_{ijk}+d_{ijk}+\phi^{(2)}_{ijk}-\epsilon_{ijk}=0. \tag{13}$$

This can be explicitly solved for the triple moment:

$$\langle u_i u_j u_k\rangle = (G_{ijk}+\tfrac{1}{3}(\beta-2)\,T[g_{ij}G_k+g_{jk}G_i+g_{ik}G_j])/3\beta T, \tag{14}$$

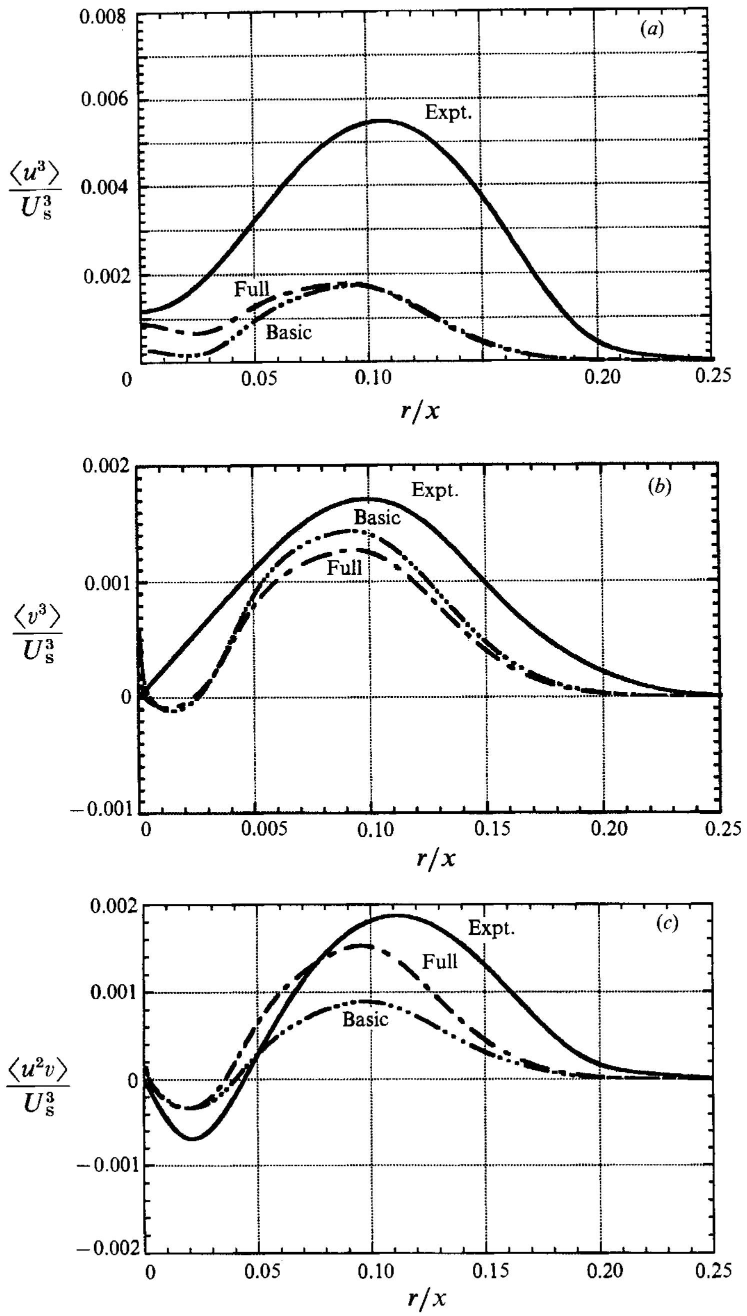

FIGURE 20 (*a–c*). For caption see facing page.

where
$$G_{ijk} = [\langle u_i u_j \rangle_{,m} \langle u^m u_k \rangle + \langle u_j u_k \rangle_{,m} \langle u^m u_i \rangle + \langle u_k u_i \rangle_{,m} \langle u^m u_j \rangle], \tag{15}$$
$$G_k = G_{ik}. \tag{16}$$

In deriving the model for the diffusion term the fourth moments have been approximated by the quasi-Gaussian approximation:

$$\langle u_i u_j u_k u^m \rangle = \langle u_i u_j \rangle \langle u^m u_k \rangle + \langle u_j u_k \rangle \langle u^m u_i \rangle + \langle u_k u_i \rangle \langle u^m u_j \rangle. \tag{17}$$

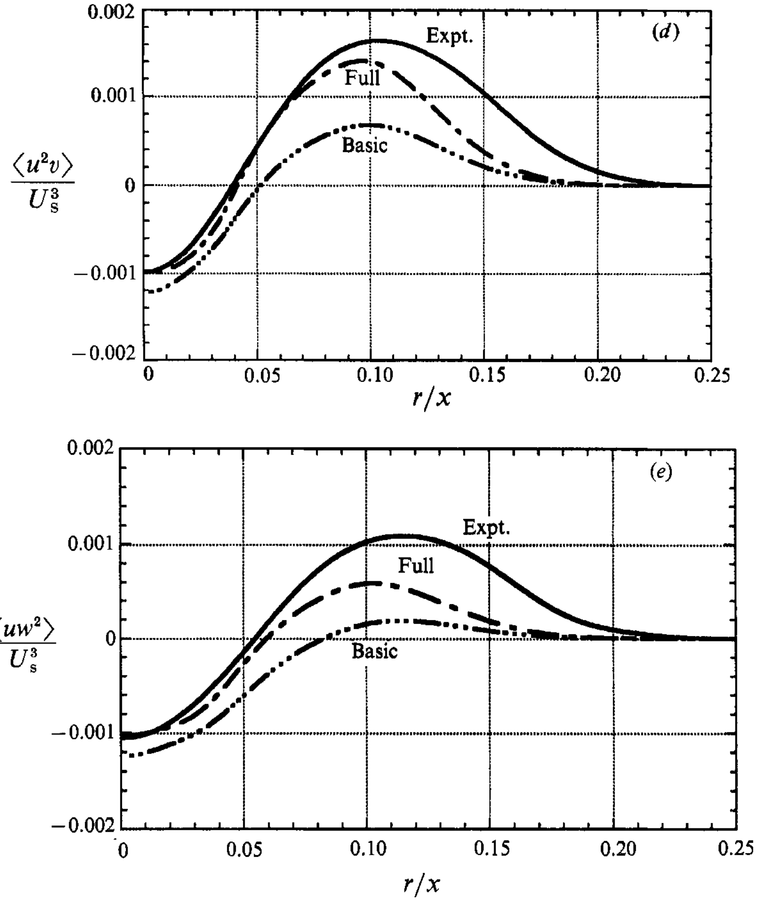

FIGURE 20. Comparison of predictions of *Basic* and *Full* models (refer to §4.3 for description) with experimental measurements for (*a*) $\langle u^3\rangle$, (*b*) $\langle v^3\rangle$, (*c*) $\langle u^2v\rangle$, (*d*) $\langle uv^2\rangle$, (*e*) $\langle uw^2\rangle$.

In the intermittent region of the jet, $\eta > 0.1$, turbulence is not quasi-Gaussian, yet the above approximation describes fourth moments very well over the entire jet as can be seen from figure 18, where $\langle u^3v\rangle$ and $\langle u^2w^2\rangle$ are shown along with the quasi-Gaussian approximation. All other fourth moments measured show a similar good agreement.

Neglect of advection, mean-strain production and rapid pressure terms in deriving the above model has been justified with the fine-grained turbulence assumption. However, most turbulent shear flows are not fine-grained. The budget for triple moment $\langle u^2v\rangle$ shown in figure 19 confirms this: the mean-strain production term is just as large in magnitude as the turbulent production term. The mean-strain production term is small for some third moments while the advection term is found to be negligible for all third moments. This indicates that the neglect of mean-strain production and rapid pressure correlations may not be justified in shear flows. Figure 19 also shows that the estimate of diffusion from measured fourth moments agrees fairly well with that obtained from the quasi-Gaussian approximation for the fourth moments.

Inclusion of mean-strain production terms does not require additional modelling.

The rapid pressure terms, however, do need to be modelled and a simple model, linear in triple moments, is described in Lumley (1978) and Lumley (1981):

$$-\langle p^{(1)}_{,1} u_j u_k\rangle/\rho = 2UP_{,q}(\tfrac{2}{5}g_{pi}\langle u^q u_j u_k\rangle - \tfrac{1}{10}(g_p q\langle u_i u_j u_k\rangle + g_i q\langle u_p u_j u_k\rangle)). \quad (18)$$

When the models for all three terms in $\phi^{(1)}_{ijk}$ are combined and added to the mean-strain production ter, $P^{(\mathrm{M})}_{ijk}$, the result is

$$\phi^{(1)}_{ijk} + P^{(\mathrm{M})}_{ijk} = \tfrac{2}{5}(S^m_i\langle u_m u_j u_k\rangle + S^m_j\langle u_i u_m u_k\rangle + S^m_k\langle u_i u_j u_m\rangle), \quad (19)$$

where S^i_j is the mean strain rate, $\frac{1}{2}(U^i_{,j} + U^j_{,i})$. The model for triple moments which includes these two terms is given by

$$P^{(\mathrm{T})}_{ijk} + P^{(\mathrm{M})}_{ijk} + d_{ijk} + \phi^{(1)}_{ijk} + \phi^{(2)}_{ijk} - \epsilon_{ijk} = 0. \quad (20)$$

This represents a system of coupled linear algebraic equations for the triple moments and will be denoted as the *Full* model.

Comparisons of model calculations with measured third moments are shown in figure 20. The performance of the *Basic* model is poor for all moments. In the fully turbulent region, $0 < \eta < 0.1$, the predictions of the *Full* model compare very well with measurements for $\langle u^2 v\rangle$, $\langle uv^2\rangle$, $\langle uw^2\rangle$ and to some extent for $\langle v^3\rangle$. The *Full* model underpredicts all moments in the intermittent region and underpredicts $\langle u^3\rangle$ throughout. both *Basic* and *Full* models predict the shapes of all triple moments very well including the negative regions near the axis. The disagreement in the intermittent region is to be expected because the assumptions made in deriving the models are violated in that region. The disagreement is not due to the inadequacy of the quasi-Gaussian approximation for the diffusion terms or due to the neglect of advection. It is the modelling of the pressure correlations and the dissipation term that is unsatisfactory. Admittedly the rapid pressure model used is very simple, being linear in third moments. Similar linear models for second-order quantities have been found to be unsatisfactory. An extension of second-order modelling ideas to intermittent flows (see Chen 1985) uses the same model for triple moments but with conditional averages for the turbulent zone substituted for unconditional averages. Turbulent zone averages were not measured in the present study.

Launder and co-workers (see Dekeyser & Launder 1983) have proposed several models for triple moments that are easier to implement. The model known as the Hanjalic and Launder model (H–L) is given by

$$\langle u_i u_j u_k\rangle = -\tfrac{1}{2}Tc_s G_{ijk}; \quad c_s = 0.11, \quad (21)$$

which is similar to the *Basic* model described above with the dissipation term neglected. Dekeyser & Launder (1983) describe a more elaborate scheme to close the third-moment equation and suggest the following models for the different terms:

$$\phi^{(1)}_{ijk} = -0.5P^{(\mathrm{M})}_{ijk}, \quad (22a)$$

$$\phi^{(2)}_{ijk} = -\frac{2}{c}\frac{\langle u_i u_j u_k\rangle}{T} - 0.5P^{(\mathrm{T})}_{ijk}; \quad c = 0.075, \quad (22b)$$

$$\epsilon_{ijk} = -\tfrac{1}{2}Tc_\epsilon \epsilon_{,m}(\langle u_k u^m\rangle g_{ij} + \langle u_j u^m\rangle g_{ki} + \langle u_i u^m\rangle g_{jk}); \quad c_\epsilon = 0.2. \quad (22c)$$

(The models given above for the pressure terms are specified to be only for the non-dispersive part. As the pressure diffusion is neglected in their models we may use the same notation.) These models can be put together along with the quasi-Gaussian

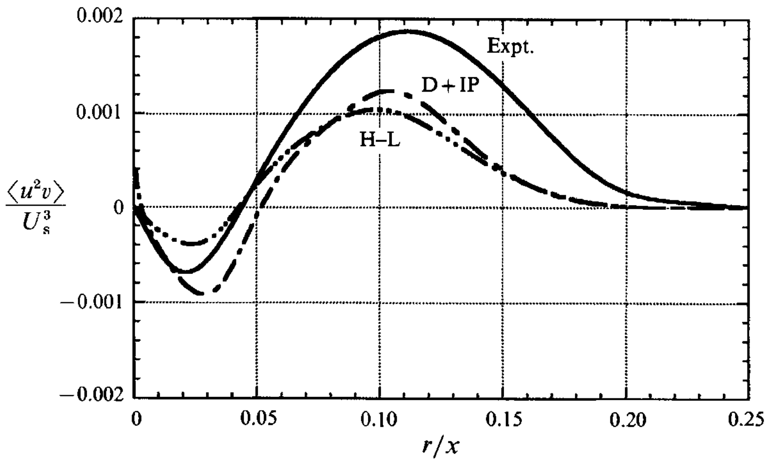

FIGURE 21. Comparison of predictions of Hanhalic and Launder model (H–L) and Dissipation + Isotropization model (D + IP) with measurements for the triple moment $\langle u^2v\rangle$.

approximation for the diffusion term d_{ijk}, to get what we shall call the D + IP model (Dissipation + Isotropization of Production model) for the triple moments:

$$P_{ijk}^{(T)}+P_{ijk}^{(M)}+d_{ijk}+\phi_{ijk}^{(1)}+\phi_{ijk}^{(2)}-\epsilon_{ijk}=0. \tag{23}$$

This is of the same form as the *Full* model given above and neglects only advection. Comparison of these two models with experimental data for $\langle u^2v\rangle$ is shown in figure 21. The performance of the H–L model is comparable to that of the *Basic* model, with the D + IP model doing only slightly better. The ratio $\langle u_i u_j u_k\rangle/(-TG_{ijk})$, calculated from experimental data for different third moments, away from regions where either the numerator or the denominator is zero, shows a wide range of variation. It seems unlikely that the value of c_s can be optimized to improve the description of third moments by the H–L model for this flow.

5. Conclusions

Turbulent transport plays a dominant role in the energetics of many flows and it is important to account for it accurately in any prediction scheme. In the present study we have characterized turbulent transport in the round jet with experimental measurements made with a shuttle-mounted ×-wire hot-wire probe. The measurements are consistent with the moment equations of turbulence. Momentum flux across the jet is seen to be conserved to within ±5% of nozzle input and radial diffusive flux integrates to zero across the jet.

Hot-wire measurements made with a moving probe have detected some new features, which appear in the LDA measurements of CHG also: off-axis peak in u' and regions of negative correlations in $\langle u^2v\rangle$, $\langle uv^2\rangle$ and $\langle uw^2\rangle$. The stationary hot-wire measurements of both W & F and CHG have failed to detect these features, which are present in the fully turbulent region of the jet. The local turbulence intensity experienced by the stationary probe is lowest in the core of the jet and is comparable to that experienced by the moving hot-wire probe (28% and 18%) and the probability of rectification and drop-out errors in this region is close to zero. This raises serious questions about measurement of higher-order moments by stationary hot-wire probes. Turbulent transport is determined by the gradients of the triple moments and the negative regions found in the triple correlations significantly alter the picture of energy budget.

Although the moving hot-wire measurements agree qualitatively with LDA measurements of CHG in all respects, there are some systematic differences. LDA values for turbulent intensities are higher by as much as 50% in the edge region of the jet. For third moments the two agree with each other near the axis and in the edge region of the jet but the LDA measurements are higher in between. The profiles are wider for moving hot-wire and LDA measurements in comparison with stationary hot-wire measurements, indicating the extent to which stationary hot-wire measurements are affected by the rectification of signals due to flow reversals and drop-outs.

The values of turbulent intensities on the axis in the present study are significantly lower than those of W & F, Rodi, CHG-LDA and CHG-SHW, all of which were made in jets with a Reynolds number of 10^5 whereas the present Reynolds number is 1.1×10^4. Values reported by Browne *et al.* (1989) in the near field ($x/d = 15$) for a jet of Reynolds number 1.77×10^4 concur with the present measurements at $x/d = 30$. Whether this is a manifestation of a Reynolds number effect or not needs to be clarified.

Models for triple moments currently used in many prediction schemes are even simpler than the *Basic* model of Lumley and the H–L model described above, retaining only the dominant G_{ijk} term in the H–L model. In view of the failure of the *Basic* and H–L models to describe the triple moments in the jet adequately this practice needs to be re-examined. The use of the simpler model has been justified by citing the computational complexity introduced by the algebraic coupling of more elaborate models. That this coupling cannot be avoided is made clear by the relative importance of the mean-strain production as seen from the budget for triple moments and by the success of the *Full* model in the fully turbulent region. Predictions of triple moments in the intermittent region are not satisfactory and indicate that the models for pressure effects and dissipation need to be improved. The need for a correct description of turbulent transport is also emphasized by the component energy budgets. The predictions for the triple moment of axial velocity fluctuations $\langle u^3 \rangle$ is much lower than measured values. Though this represents only an axial flux and hence is not dynamically important, consistent underprediction in regions of negligible gradients of normal stresses needs attention.

We wish to thank Professor W. K. George for providing us with reports of work done at University at Buffalo, SUNY, Mr E. P. Jordan for his invaluable assistance in all aspects of experimental work, especially for the fabrication and operations of the shuttle, and Professor Warhaft, Mr R. Ristorcelli, Mr A. Poje, Mr P. C. Miles and Dr S. Veeravalli for their comments on the final form of the paper. This work was supported in part by US Office of Naval Research, Fluid dynamics and Power program (N00014-79-C-0482) and by NASA Langley, Hypersonic Turbulence Modelling Program (NAG-1-954).

REFERENCES

Browne, L. W. B., Antonia, R. A. & Chua, L. P. 1989 Calibration of × -probes for turbulent flow measurements. *Expts Fluids* **7**, 201–208.

Capp, S. P. 1983 Experimental investigation of turbulent axisymmetric jet. PhD dissertation, University at Buffalo, SUNY.

Capp, S. P., Hussein, H. J. & George, W. K. 1990 Velocity measurements in a high Reynolds number, momentum-conserving, axisymmetric, turbulent jet. *Tech. Rep.* 123. Turbulence Research Laboratory, University at Buffalo, SUNY (referred to herein as CHG).

Chen, J. 1985 Second-order modeling of turbulent reacting flows with intermittency and conditional averaging. PhD dissertation, Cornell University, Ithaca.

Dekeyser, I. & Launder, B. E. 1983 A comparison of triple-moment temperature-velocity correlations in the asymmetric heated jet with alternative closure models. In *Turbulent Shear Flows 4* (ed. L. J. S. Bradbury *et al.*). Springer.

Duncan, B. S., Lumley, J. L., Shih, T. H. & To, W. M. 1992 A new model for the turbulent dissipation. In *Proc. Intl Conf. of Fluid Mechanics and Theoretical Physics. Beijing, PRC.* Chinese Society for Theoretical and Applied Mechanics. (Also Report No. FDA-92-08, Sibley School of Mechanical and Aerospace Engineering. Ithaca, NY: Cornell.

George, W. K., Capp, S. P., Seif, A. A., Baker, C. B. & Taulbee, D. B. 1988 A study of the turbulent axisymmetric jet. *J. Engng Sci. King Saud Univ.* **14**, 85–93.

Gouldin, F. C., Schefer, R. W., Johnson, S. C. & Kollmann, W. 1986 Nonreacting turbulent mixing flows. *Prog. Energy Combust. Sci.* **12**, 257–303.

Hussein, H. J. 1988 Measurements of small scale turbulence in an axisymmetric jet using moving hot wires. PhD dissertation, University at Buffalo, SUNY.

Hussein, H. J. & George, W. K. 1990 Locally axisymmetric turbulence. *Tech. Rep.* 122. Turbulence Research Laboratory, University at Buffalo, SUNY.

Lueptow, R. M., Breuer, K. S. & Haritonidis, J. H. 1988 Computer-aided calibration of ×-probes using a look-up table. *Exps Fluids* **6**, 115–118.

Lumley, J. L. 1978 Computational modelling of turbulent flows. *Adv. Appl. Mech.* **18**, 123–176.

Lumley, J. L. 1981 Parametrization of turbulent transport in swirling flows. *FDA Rep.* 81-02. Sibley School of Mechanical and Aerospace Engineering, Cornell University, Ithaca.

Panchapakesan, N. R. & Lumley, J. L. 1993 Turbulence measurements in axisymmetric jets of air and helium. Part 2. Helium jet. *J. Fluid Mech.* **246**, 225–247.

Ricou, F. P. & Spalding, D. B. 1961 Measurements of entrainment by axisymmetrical turbulent jets. *J. Fluid Mech.* **11**, 21–32.

Rodi, W. 1975*a* A new method of analyzing hot-wire signals in highly turbulent flow and its evaluation in a round jet. *DISA Information* 17, *Feb.* 1975.

Rodi, W. 1975*b* A review of experimental data of uniform density free turbulent boundary layers. In *Studies in Convection*, Vol. 1 (ed. B. E. Launder). Academic.

Seif, A. A. 1981 Higher order closure model for turbulent jets. PhD Dissertation, University at Buffalo, SUNY.

Taulbee, D. B. 1988 Engineering turbulence models. In *Advances in Turbulence* (ed. W. K. George & R. E. A. Arndt). Hemisphere.

Taulbee, D. B., Hussein, H. & Capp, S. 1987 The round jet: experiment and inferences on turbulence modeling. In *Sixth Symp. on Turbulent Shear Flows, Toulouse, France.* Paper 10-5-1.

Tennekes, H. & Lumley, J. L. 1972 *A First Course in Turbulence.* MIT Press.

Wygnanski, I. & Fiedler, H. 1969 Some measurements in the self-preserving jet. *J. Fluid Mech.* **38**, 577–612 (referred to herein as W & F).